A physical model investigation of P and S wave azimuthal anisotropy on transmission

Khaled Al Dulaijan, Gary Margrave, and Joe Wong

ABSTRACT

Information related to fracture orientation and intensity is vital for the development of unconventional hydrocarbons, such as tight sand gas and shale gas. Numerical modeling provides a valuable tool for geophysicists to test and validate their methodologies that provide them with information about reservoirs. Fractures make numerical modeling more complicated and introduce complexities that might even require geophysicists to validate their numerical models before using them to test and validate their methodologies. Alternatively, physical modeling provides a unique opportunity to test, validate, and develop methods for characterizing fractured reservoirs. This report utilizes seismic physical modeling for fracture characterization, is a continuation to previous work conducted within CREWES, and is an in-progress work.

A two-layer model was built using vertically laminated Phenolic overlaid by Plexiglas to represent a fractured reservoir overlaid by an isotropic overburden. Three 9-component common-receiver gathers were acquired over that model in the laboratory. For each gather, 90 shot locations are distributed along a circle of radii 250 m, 500 m, or 1000 m and separated by 4° to cover all azimuths. P-wave first-arrival times were analyzed on all three gathers and fracture orientation was predicted. S-wave analysis suggests an error in the polarization direction of the horizontal transducers. An Alford rotation was applied to the four horizontal components and successfully minimized energy on components other than those two that have fast S wave and slow S wave.

INTRODUCTION

Understanding fracture orientation and intensity is often challenging, yet important for the optimal development for fractured reservoirs. Fractures can act as conduits for fluid flow. Seismic anisotropy can assist in understanding fractures, even though sometimes it is related to the regional stress regime. In this report, we are interested in fracture-induced seismic anisotropy, and more specifically in vertical fractures or Horizontal-Transverse Isotropy (HTI). Azimuthal anisotropy makes numerical modeling hard and introduces uncertainties. On the other hand, physical modeling provides a reliable alternative. This report is a continuation to previous CREWES work (e.g. Wong et al., 2012; Mahmoudian 2013; Mahmoudian and Margrave 2013) that utilizes physical modeling.

In the physical modeling laboratory, a fractured reservoir and isotropic overburden can be represented by a two-layer (anisotropic and isotropic) model. Because azimuthal anisotropy is of interest to us, we want to acquire gathers of common offset and varying azimuth angles. In such a way, fracture orientation can be predicted from azimuthal analysis of P-wave first arrival times. Also, it can be predicted by S-wave splitting

because fast S wave polarization direction indicates directly the orientation of fractures. Sometimes, a four-component horizontal rotation (i.e. Alford rotation) is needed to separate fast S wave from slow S wave.

PHYSICAL MODELING

A physical model was created to represent a vertically fractured reservoir overlaid by isotropic overburden, as shown in Figure 1. The vertically fractured reservoir exhibits an HTI type anisotropy, or more precisely slightly orthorhombic anisotropy (Mahmoudian, 2013). For VTI or HTI anisotropy, Phenolic material can be used. Vertically laminated sheets of linen fabric bonded with Phenolic resin compose the Phenolic HTI medium (Figure 2).

FIG. 1. A physical model consisting of a Phenolic layer under a Plexiglas layer, and representing a fractured reservoir overlaid by isotropic overburden. Laboratory to field scale is 1:10,000 in both length and time. Scaled thicknesses of Plexiglas and Phenolic layers are 480 m and 450 m respectively.
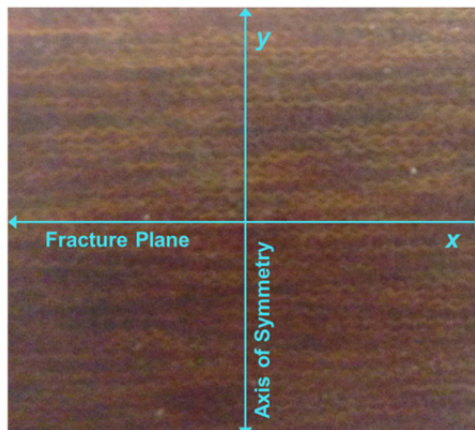

FIG. 2. A zoomed-in surface view of laminated Phenolic layer. Lamination direction is along x-axis and represents the reservoir fracture plane. Axis of symmetry is along y-axis.

In the Phenolic medium, P wave is fastest (3570 m/s) along the vertical laminations, slowest (2900 m/s) perpendicular to the vertical lamination, and somewhere in between along other directions. On the other hand, S wave is fastest (1700 m/s) along the vertical laminations, slowest (1520 m/s) perpendicular to the vertical lamination, and undergoes S-wave splitting in other direction. The isotropic overburden was represented by Plexiglas. P-wave and S-wave velocities in the isotropic medium are 2745 m/s and 1520 respectively. Properties of Phenolic and Plexiglas are summarized in Table 1 (Mahmoudian, 2013).

	P-wave velocity (m/s)	S-wave velocity (m/s)	Density (g/cc)
Plexiglas	2745	1380	1.19
Phenolic	3570/2900	1700/1520	1.39

Table 1. Velocities and densities of Plexiglas and Phenolic.

The laboratory to field scale is 1:10,000 in both length and time. Scaled thicknesses of Plexiglas and Phenolic layers are 480 m and 450 m respectively. The acquisition layout is illustrated in Figure 3. Three common-receiver gathers were acquired. One receiver location was fixed at the bottom of the Phenolic layer and centered at the middle of its surface. For each common-receiver gather, 90 source locations were distributed along a circle of radius (r) and separated by 4°. Three receiver gathers were acquired with r = 250 m, 500 m and 1000 m. 3-C receiver and 3-C source yield into 9-component receiver gathers.

Contact transducers were used as P-wave and S-wave sources and receivers (Figure 4). Those transducers are 6 mm thick. P-wave transducers have a central frequency at 2.38 MHz, while S-wave transducers have central frequency at 5.82 MHz. In each station (source/receiver), three transducers were used; once for vertical component and then twice for horizontal components along x- and y-axes. Source and receiver transducers were positioned with a robotic system that has an error of less than 0.1 mm laboratory scale.

DATA ANALYSIS

Three common-receiver gathers of r = 250 m, 500 m and 1000 m are shown in Figures 5-7. Each gather (v) is composed of 9 components. The first subscript of v denotes the receiver component, while the second subscript denotes the source component. *x*-, *y*-, and *z*-components are labeled by the numbers *1*, *2*, and *3* respectively. For example, v_{31} was acquired with a vertical receiver and a source along the *x*-axis.
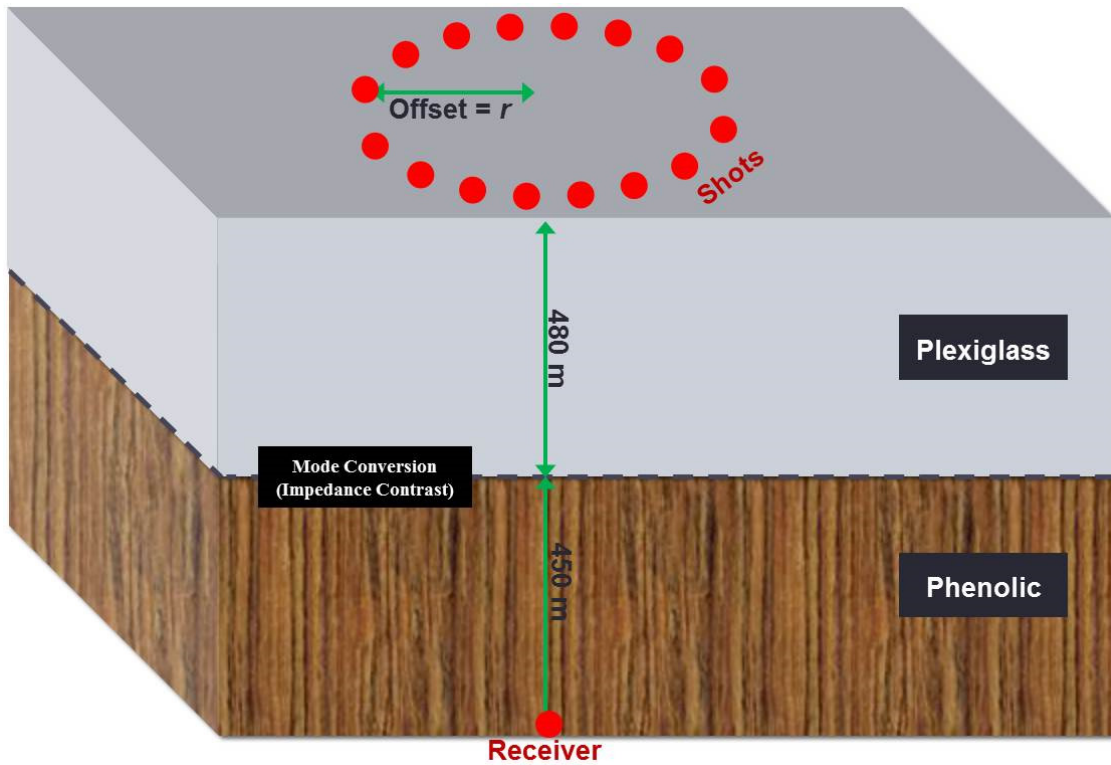
FIG. 3. Acquisition layout. One receiver location is located at the bottom of the Phenolic layer and centered at the middle of its surface. 90 shot locations are distributed along a circle of radius (*r*) and separated by 4°. Three receiver gathers are acquired with r = 250 m, 500 m and 1000 m. 3-C receiver and 3-C source yield into 9-C receiver gathers.
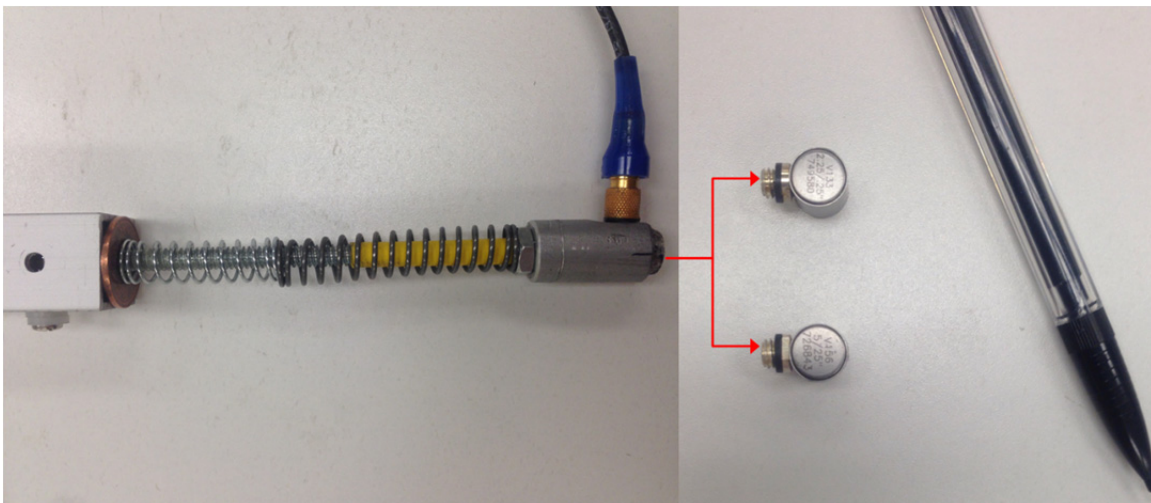

FIG. 4. Positioning arms with a contact transducer connected to the right end (left). P-wave and S-wave transducers (right)
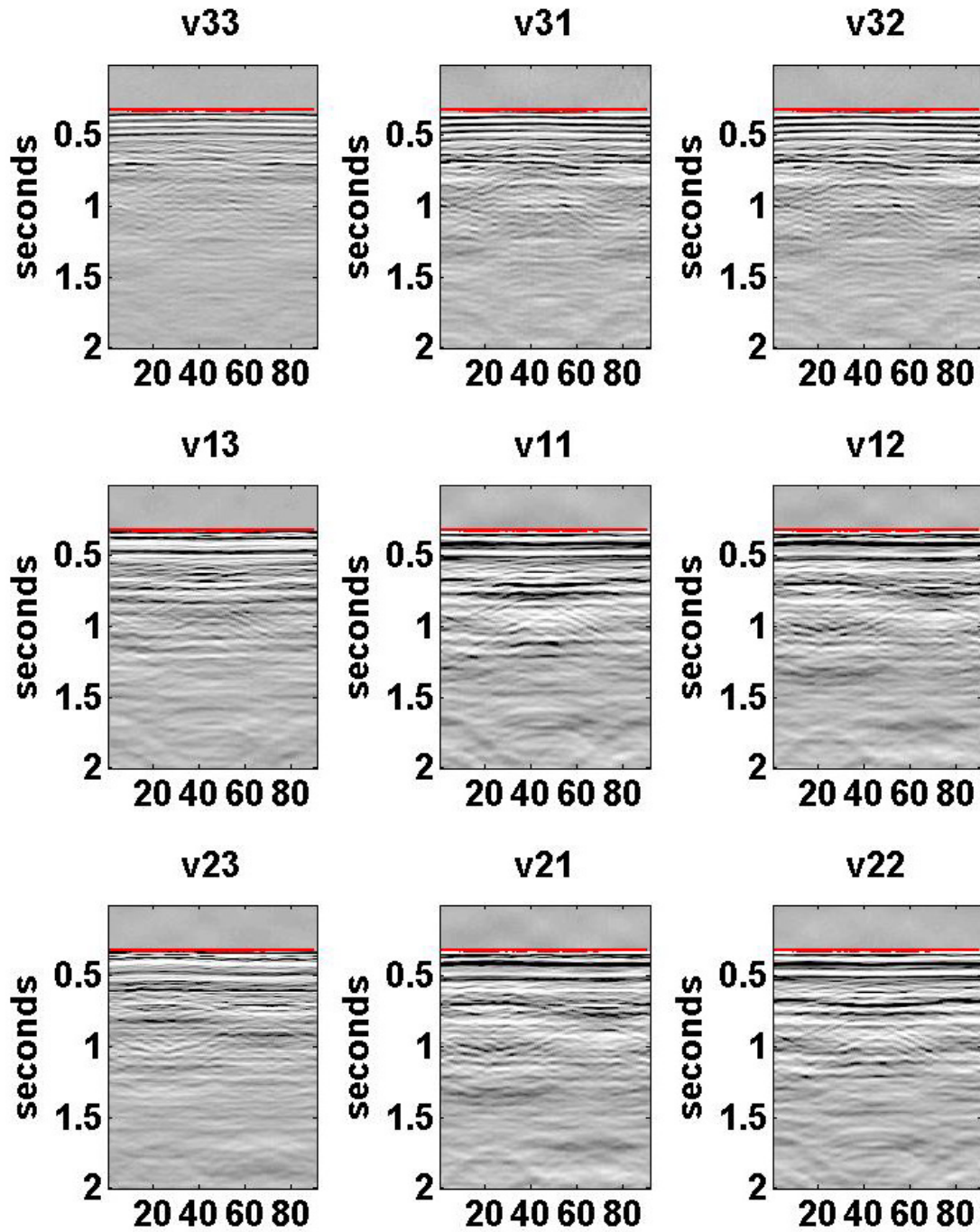
FIG. 5. 9-C receiver gather with **r** = 250 m. P-wave first arrival times are indicated by red. The horizontal axis is the trace number. Traces 1 to 90 represent azimuth angles from 0° to 360° with a 4° increment.

FIG. 6. 9-C receiver gather with **r** = 500 m. P-wave first arrival times are indicated by red. The horizontal axis is the trace number. Traces 1 to 90 represent azimuth angles from 0° to 360° with a 4° increment.
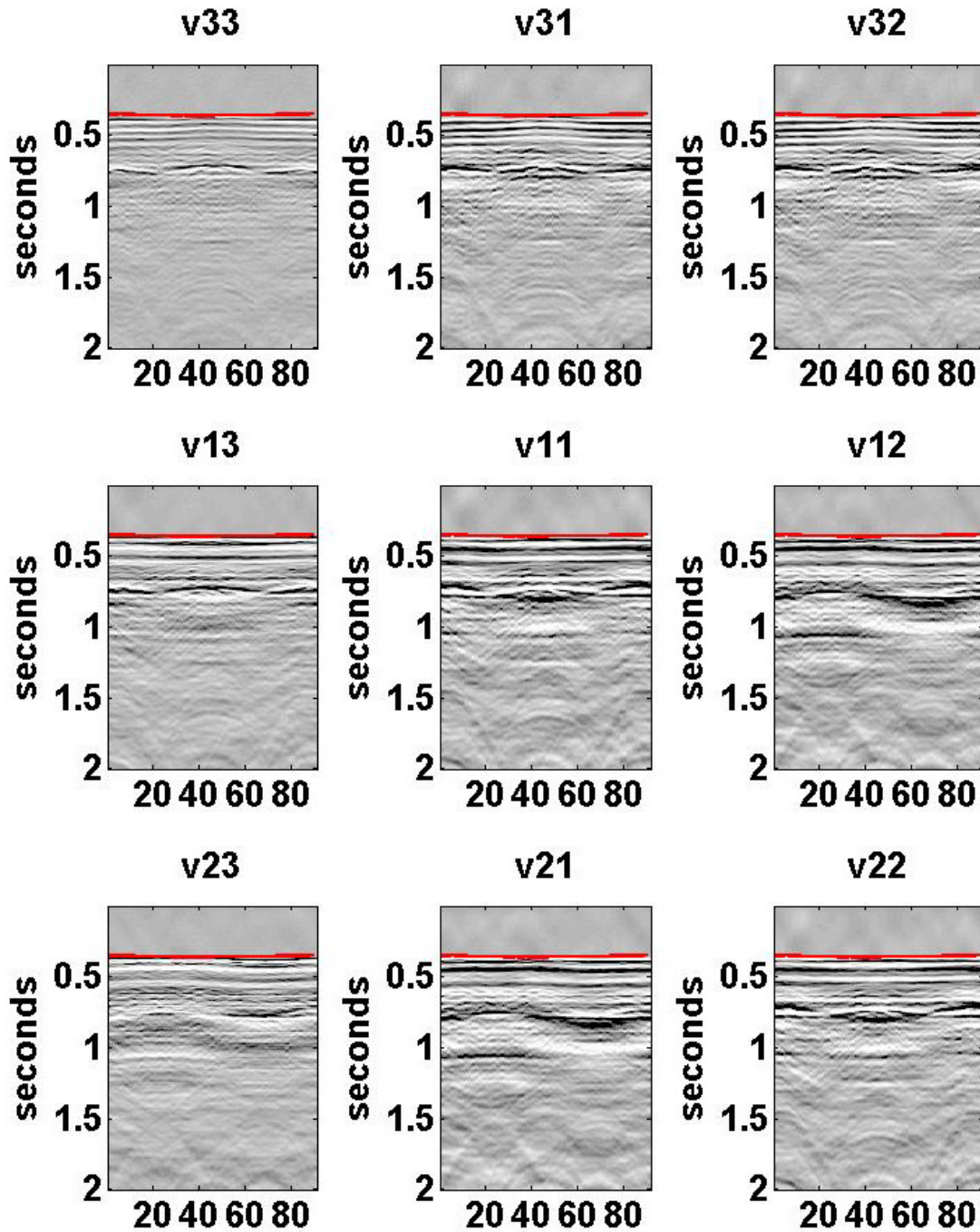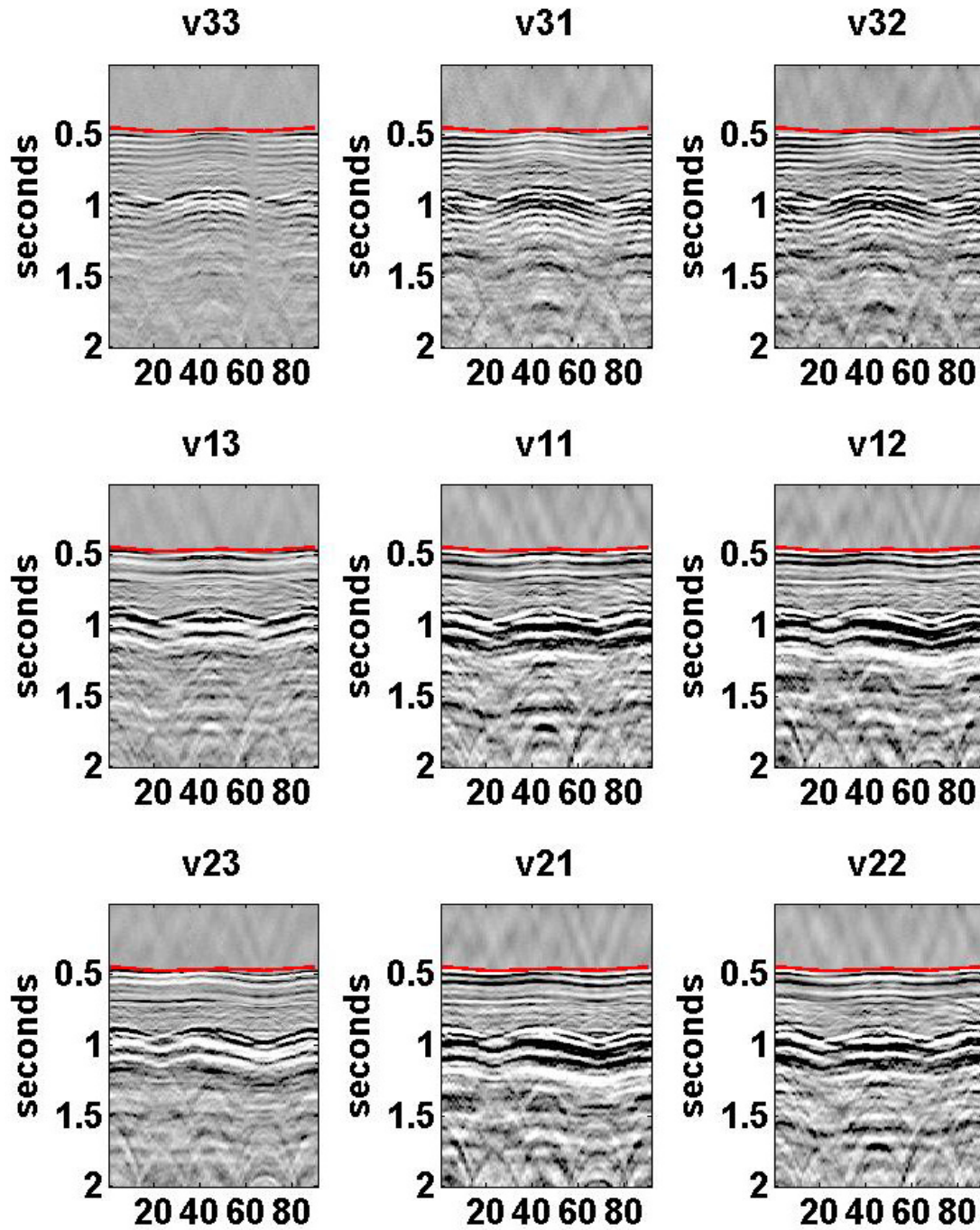
FIG. 7. 9-C receiver gather with **r** = 1000 m. P-wave first arrival times are indicated by red. The horizontal axis is the trace number. Traces 1 to 90 represent azimuth angles from 0° to 360° with a 4° increment.

The three common-receiver gathers in Figures 5-7 are plotted with the same amplitude range. Azimuth goes from 0° to 360° with an increment of 4° for the 1st to the 90th trace. First arrival times were picked on onset and indicated by red. The 250-m and 500-m common-receiver gathers show nearly constant first-arrival times with increasing azimuth angle. The 1000-m common-receiver gather show a sinusoidal variation of first arrival times with increasing azimuth angle. The acquisition layout suggests that components v_{11} of the three gathers in Figures 5-7 are acquired with horizontal receivers and sources along the *x*-axis or parallel to fracture plane. Similarly, v_{22} components have transducer polarization perpendicular to fracture plane.

P-wave first-arrival times analysis

In isotropic media, P-wave first-arrival times are constant for the same offset and different azimuths. Each common-receiver gather in Figures 5-7 has a constant offset. Figure 7 shows first-arrival times that are variant with azimuth angle and look like a sinusoidal function. Early first arrivals are at 0°, 180^0, and 360^0. Those angles define the fast P-wave direction which is parallel to the fracture plane. This result is in agreement with the physical model where fracture plane within the Phenolic is along *x*-axis, as can be seen by Figure 2. In Figures 5 and 6, it is hard to see sinusoidal first-arrival times.

If plotted azimuthally in a polar view, sinusoidal first-arrival times appear as an ellipse. The minor axis of the ellipse indicates early first-arrival times, while the major axis indicates late first-arrival times (Figure 7). Therefore, the minor axis indicates the fracture plane (Al Dulaijan et al., 2012). In Figure 7, fast direction is at 60° and the minor axis of the fitted ellipse is at the same angle.
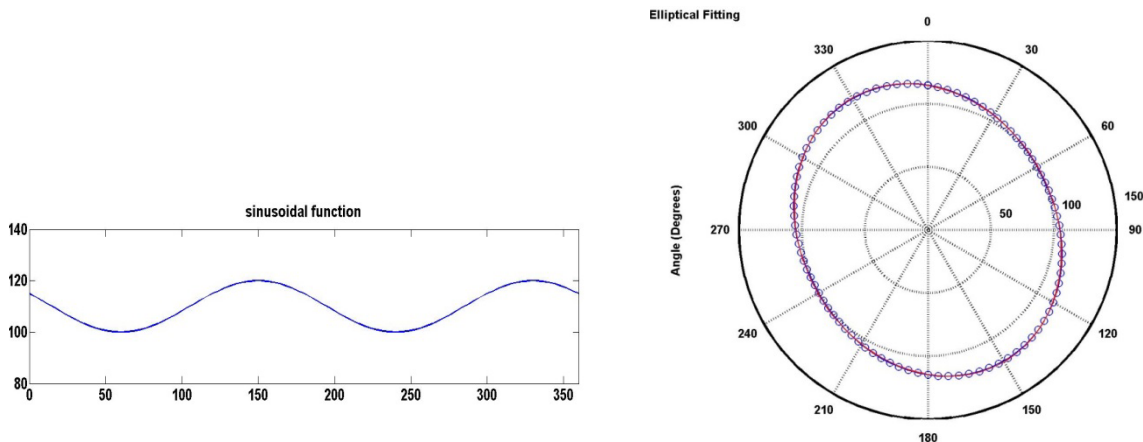

FIG. 8. A sinusoidal function representing azimuthally variant first arrival times (left). Fast direction is 60° and slow direction is 150°. Elliptical fitting of first arrival times (right). First arrival times are indicated by blue circles and fitted ellipse is indicated by red. Minor axis at 30° is the fast direction while major axis at 150^0 is the slow direction. Minor axis indicated fracture plane.

For each common-receiver gather, first-arrival times are plotted azimuthally in a polar view. Then by least-squares fitting, an ellipse is fitted. Figures 8-10 show elliptical fitting of first-arrival times for each gather. The minor axis for the first and second gather (Figures 8 and 9) is at 5°. The minor axis for the third gather is 1°. The minor axes indicate the fracture plane which is supposed to be 0° according to the physical model (Figure 2). The first and second common-receiver gathers have a smaller offset than the third gather, and therefore are more sensitive to acquisition inaccuracies.
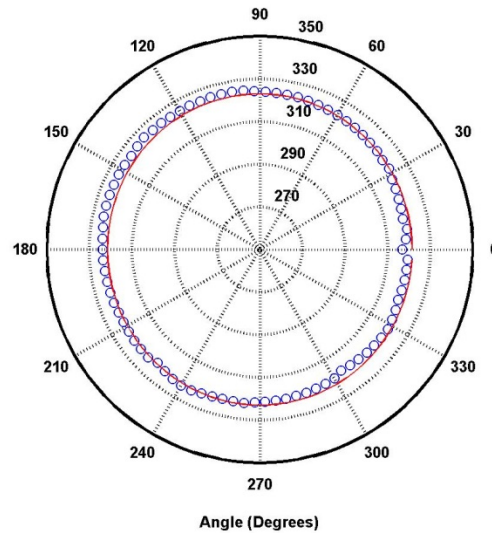

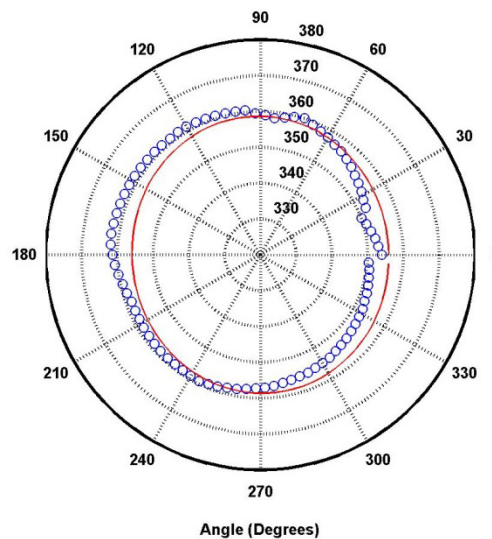FIG. 9. Elliptical fitting of first-arrival times for the first receiver gather (*r* = 250 m). The minor axis is at 5^0.

FIG. 10. Elliptical fitting of first-arrival times for the second receiver gather (*r* = 500 m). The minor axis is at 5^0.
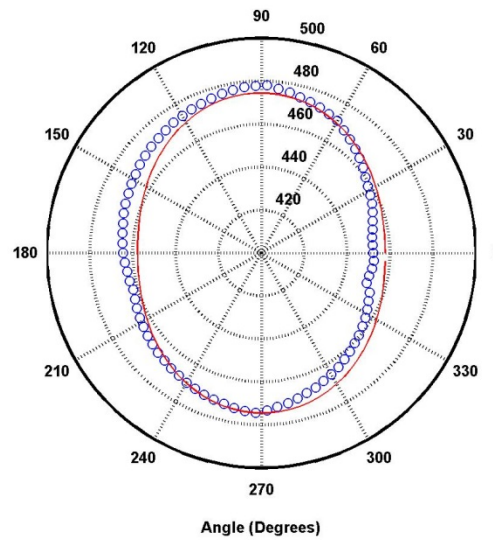
FIG. 11. Elliptical fitting of first-arrival times for the third receiver gather (*r* = 1,000 m). The minor axis is at 1^0.

S-wave splitting: Alford rotation

In HTI media, P wave is fastest along the fracture planes, slowest perpendicular to fracture planes, somewhere in between in other direction. On the other hand, S wave has to split into two phases; a phenomena known as S-wave splitting, S-wave birefringence, and S-wave double-refraction. Polarizations of the two S waves are determined by anisotropy axis of symmetry. The fast S is polarized along the fracture planes and slow S is perpendicular to the fracture planes. Beside the anisotropy axis of symmetry, the velocity of S wave is controlled also by the angle of incidence and the azimuth of propagation. The two S waves travel at different velocities (within the Phenolic) and are recorded at different times. The delay in time is proportionally related to the degree of S-wave anisotropy and thickness of the anisotropic medium (Crampin, 1981).

For all three common-receiver gathers, horizontal components of receivers and sources were aligned along *x*- or *y*-axis. In another word, they were aligned either parallel to fracture plane or normal to the fracture plane. In such a way, S wave is fast along *y*-axis and slow along *x*-axis. In other directions, S wave undergoes S-wave splitting and repolarizes along fast and slow directions. Fast S wave should mostly be recorded by v_{11} and slow S wave by v_{22}. Energy on v_{12} and v_{21} should be minimal. This was not the case in our experiment! That suggests an error in the polarization direction of the horizontal transducers.

An Alford 4-component rotation (Alford, 1986) can be used to statistically rotate horizontal components (*V*) recorded in acquisition recorded system into anisotropy natural coordinate system (*U*) using rotation matrix (*R*(θ)):

$$V = \begin{bmatrix} v_{11} & v_{12} \\ v_{21} & v_{22} \end{bmatrix}, \tag{1}$$

$$U = \begin{bmatrix} u_{11} & u_{12} \\ u_{21} & u_{22} \end{bmatrix} \tag{2}$$

, and

$$R(\theta) = \begin{bmatrix} \cos\theta & \sin\theta \\ -\sin\theta & \cos\theta \end{bmatrix} \tag{3}$$

The rotation matrix, $R(\theta)$ is an orthogonal matrix that gives the identity matrix when multiplied by its transpose or its inverse. To find a new basis of the natural coordinate system, the counterclockwise rotation by angle (θ) is

$$U = R(\theta)\, V\, R^T(\theta). \tag{4}$$

Substituting equations (1), (2), and (3) into equation (4):

$$\begin{bmatrix} u_{11} & u_{12} \\ u_{21} & u_{22} \end{bmatrix} =$$

$$\begin{bmatrix} \cos^2\theta\, v_{11} + \sin^2\theta\, v_{22} + 0.5\sin2\theta\,(v_{21}+v_{12}) & \cos^2\theta\, v_{12} - \sin^2\theta\, v_{21} + 0.5\sin2\theta\,(v_{22}-v_{11}) \\ \cos^2\theta\, v_{21} - \sin^2\theta\, v_{12} + 0.5\sin2\theta\,(v_{22}-v_{11}) & \cos^2\theta\, v_{22} + \sin^2\theta\, v_{11} - 0.5\sin2\theta\,(v_{21}-v_{12}) \end{bmatrix} \tag{5}$$

Equation (5) transforms V, horizontal components in acquisition coordinate system into the natural coordinate system (Alford, 1986).

Rotation angle (θ) is found by scanning different angle values, and then selecting the angle that minimize u_{12} and/or u_{21}. For each common-receive gathers, angles were scanned within a time window to determine the rotation angle (θ) and Alford rotation was applied. Four horizontal components of the 1st common-receiver gather that has $r =$ 250 m is shown before rotation on the left of Figure 12 and after rotation on the right of the same figure. Figure 13 shows the cross energy of different rotation angles. For this common-receiver gather, the rotation angle (θ) is 45°. Figures 14 and 16 show four horizontal components of the other two common receiver gathers ($r = 500$ m and $r = 1000$ m) before and after rotation. Figures 15 and 17 show the cross energy of different rotation angles for the same gathers. All three gathers have rotation angles around 45°. If the polarization directions of the transducers were accurate, then Alford rotation would not be needed because the rotation angle would be 0^0 and the acquisition and natural system coordinate would be identical.
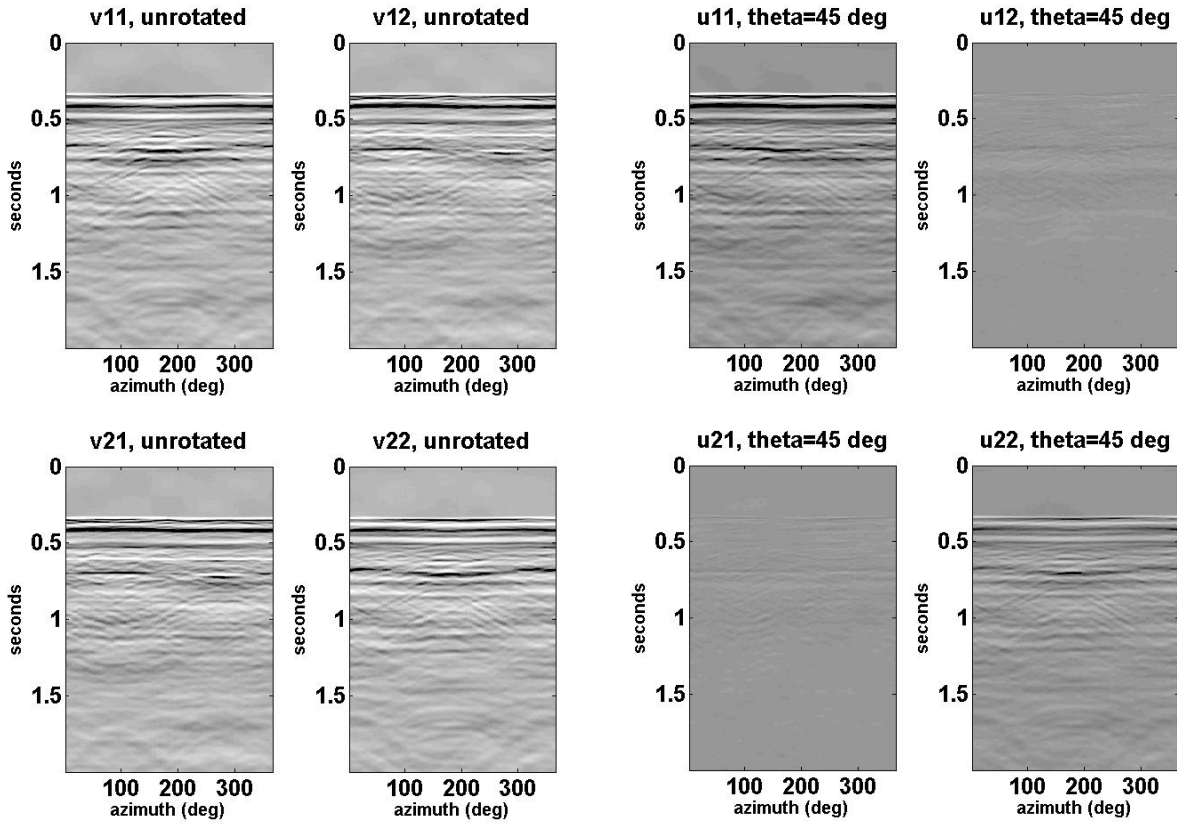
FIG. 12. 1st receiver gather: 4 Horizontal components before rotation (left) and after rotation (right).
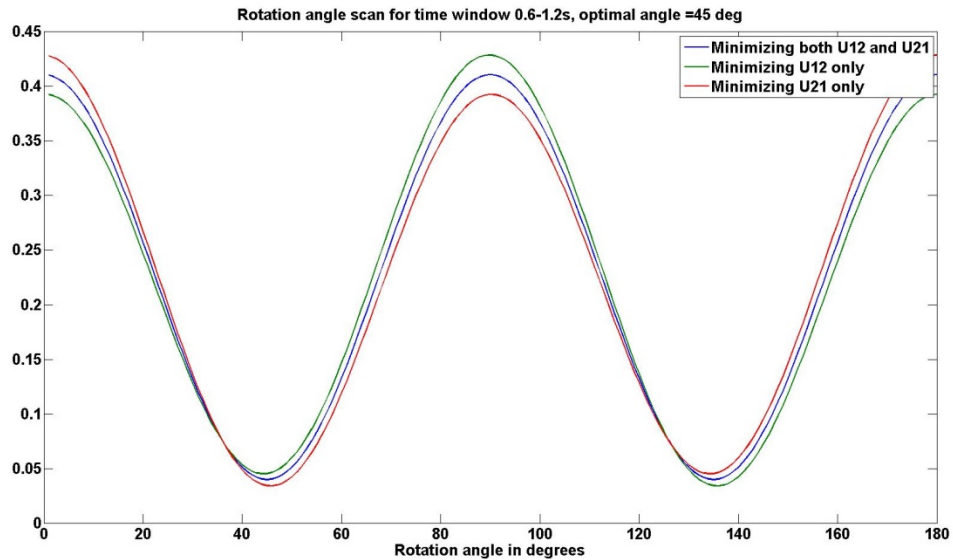

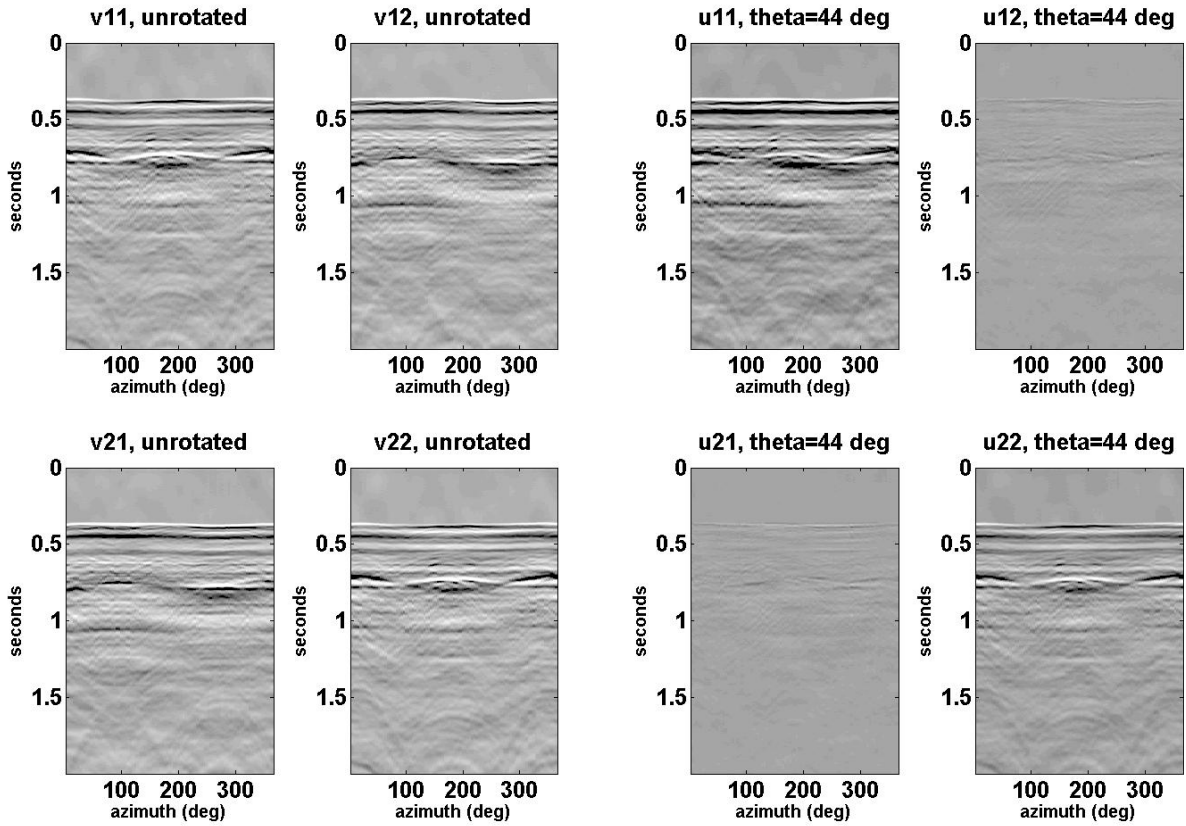FIG. 13. 1st receiver gather: cross energy vs. rotation angle.

FIG. 14. 2nd receiver gather: 4 Horizontal components before rotation (left) and after rotation (right).
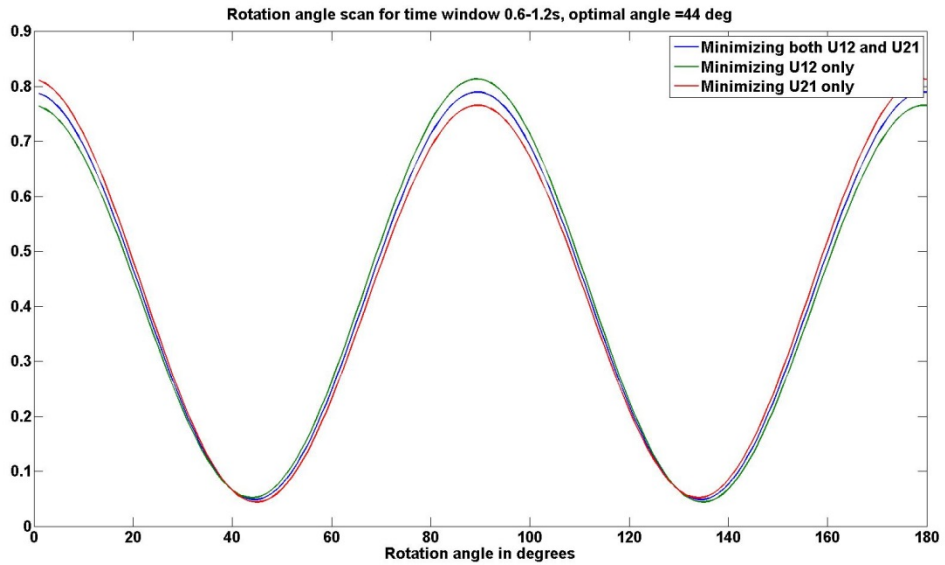

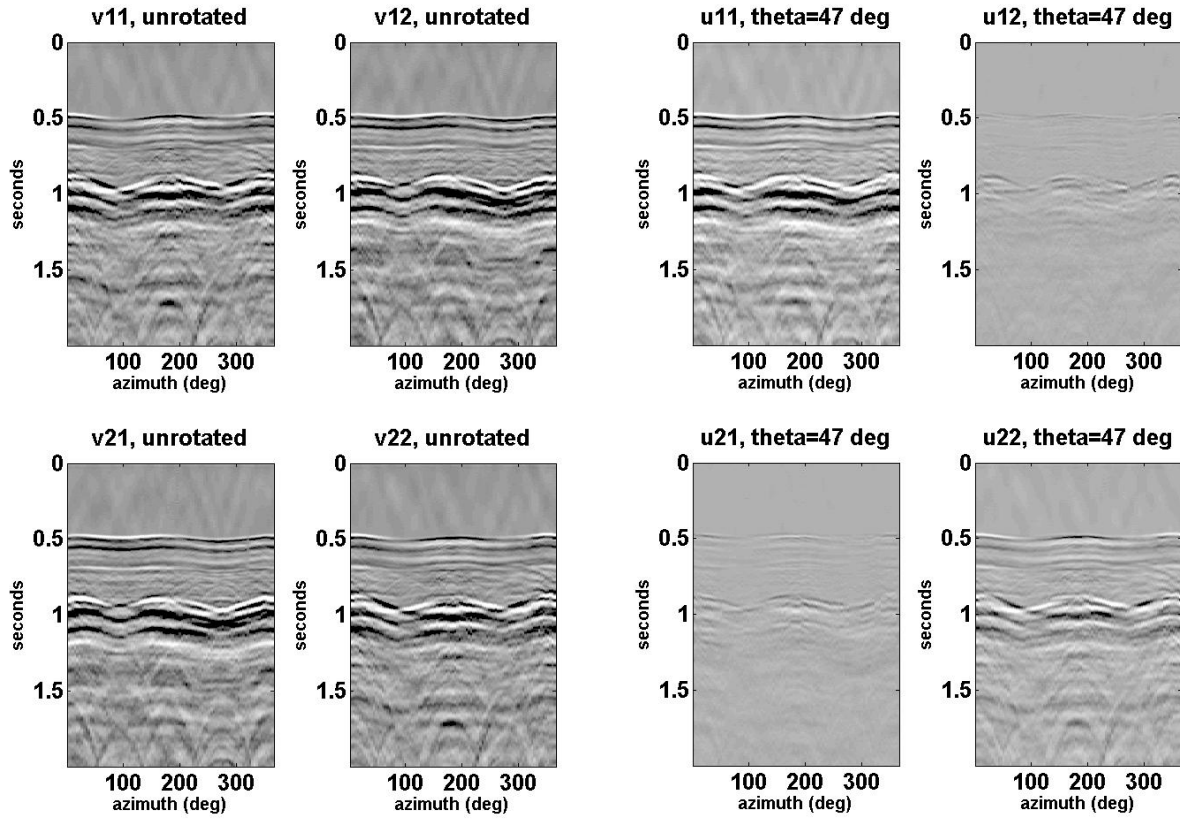FIG. 15. 2nd receiver gather: cross energy vs. rotation angle.

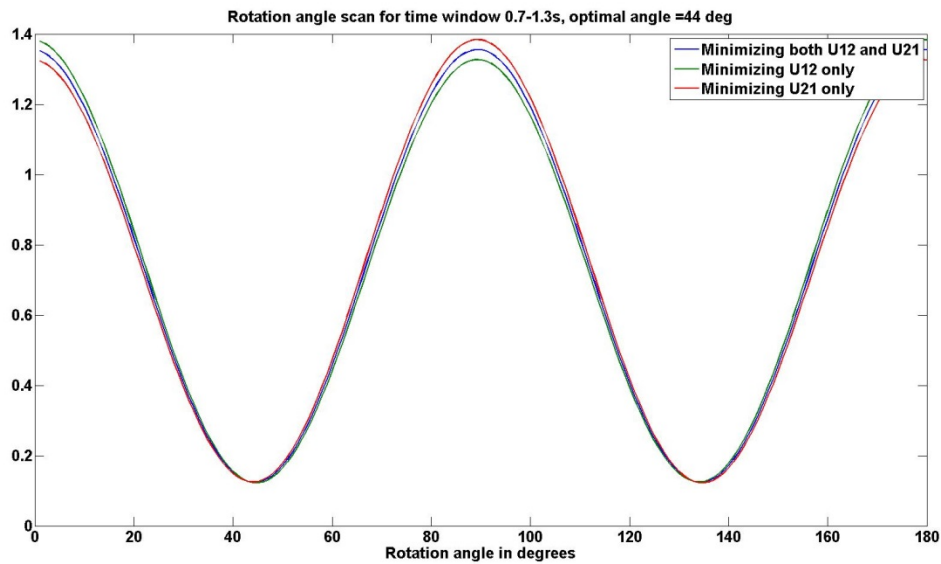FIG. 16. 3rd receiver gather: 4 Horizontal components before rotation (left) and after rotation (right).

FIG. 17. 3rd receiver gather: cross energy vs. rotation angle.

CONCLUSION

Physical modeling is a valuable tool that can assist in the evaluation and development of practices for fracture characterization. This report has utilized physical modeling, and in summary:

- A physical model was constructed in the laboratory to represent a vertically-fractured reservoir overlaid by isotropic overburden.

- Three common-receiver gathers were acquired; each has a constant offset ($r = 250$ m, 500 m and 1000 m) and variant azimuth angles (0^0- 360°).

- Fracture plane orientation was easily identified from the third common-receiver gather ($r = 1000$ m) by P-wave first-arrival times.

- Elliptical fitting of P-wave first-arrival times was employed to identify the fracture plane orientation from the three common-receiver gather.

- S-wave analysis has suggested an error in the polarization direction of the horizontal transducers.

- An Alford rotation was successfully applied to the four horizontal components of the three common-receiver gather to transform the data from acquisition system coordinate to natural system coordinate.

This report is still in progress, and currently we are planning to repeat the experiment after calibrating transducers. Also, the acquisition system coordinate will intentionally be different from the natural system coordinate, and Alford rotation will be used to predict the fracture plane orientation.

ACKNOWLEDGMENT

REFERENCES

Al Dulaijan, K., Owusu, J. C., & Weber, D. C. (2012). Azimuthal anisotropy analysis of walkaround vertical seismic profiling vertical seismic profiling: a case study from Saudi Arabia. *Geophysical Prospecting*, *60*(6), 1082-1094.

Alford, R. M., 1986, Shear data in the presence of azimuthal anisotropy: Dilley Texas, SEG Expanded Abstracts, SEG Annual Convention.

Crampin, S. (1981). A review of wave motion in anisotropic and cracked elastic-media. Wave motion, 3(4), 343-391.

Mahmoudian, F., 2013, Physical Modeling and Analysis of Seismic Data from a Simulated Fractured Medium: Ph.D. thesis, University of Calgary

Mahmoudian, F., & Margrave, G. F. (2013). AVAZ Inversion for Fracture Orientation and Intensity-A Physical Modeling Study. In 75th EAGE Conference & Exhibition incorporating SPE EUROPEC 2013.

Wong, J., F. Mahmoudian, and G. Margrave, 2011, Physical modeling III: Acquiring modeled data for VVAZ/AVAZ analysis: CREWES Research Report, 23, 1–17